Self-Unlocking Active Clutch for Quasi-Passive Wearable Robots

Jae-Ryeong Choi, *Graduate Student Member, IEEE*, Seung-Won Kim, *Member, IEEE*, and Kyu-Jin Cho, *Member, IEEE*

***Abstract*—Wearable robots have gained attention as a promising technology for enhancing human functions and capabilities. While early research focused on developing motorized exoskeletons, recent efforts have shifted toward improving wearability for user convenience. However, the size and weight of actuators and battery components in active wearable robots remain significant challenges. As an alternative, passive wearable robots using nonmotorized mechanical components are lightweight and energy-efficient, but they have limitations in adapting to different situations. This article introduces a self-unlocking active clutch (SuAC) for quasi-passive wearable robots, which combines the benefits of both active and passive systems. The SuAC utilizes a shape memory alloy coil spring and an encoder to actively lock and provide assistive force based on the user's movement. Once in a locked state, the clutch can automatically unlock when the assistive force falls below a certain threshold, based on the user's preprogrammed intentions. This self-unlocking feature eliminates the need for additional mechanical triggering components or external sensors. The SuAC weighs approximately 50 grams and can withstand a locking torque of over 500 N, with a fast response time of less than 0.15 s. To demonstrate its application, we applied the SuAC to a neck-assist exosuit, showing that the assistive force can be controlled solely by the user's movements. This research simplifies the design and expands the functionality of quasi-passive wearable robots, providing a more accessible and efficient solution for assistive technology.**

***Index Terms*—Active clutch, quasi-passive wearable robots, self-unlocking mechanism.**

Received 7 August 2024; revised 14 September 2024 and 17 October 2024; accepted 26 November 2024. Recommended by Technical Editor R. Carloni and Senior Editor D. Chen. This work was supported in part by the Korea Health Technology R&D Project through the Korea Health Industry Development Institute (KHIDI), funded by the Ministry of Health & Welfare, Republic of Korea under Grant HI19C1352, in part by the National Research Foundation of Korea(NRF) funded by the Korean Government (MSIT) under Grant RS-2023-00208052, and in part by the Korea Institute of Science and Technology institutional program under Grant 2E32983. *(Corresponding authors: Kyu-Jin Cho; Seung-Won Kim.)*

Jae-Ryeong Choi and Kyu-Jin Cho are with the Department of Mechanical Engineering and Institute of Advanced Machines and Design, Seoul National University, Seoul 08826, Republic of Korea (e-mail: jae.choi@snu.ac.kr; kjcho@snu.ac.kr).

Seung-Won Kim is with the Intelligence and Interaction Research Center, Advanced Materials and Systems Research Division, Korea Institute of Science and Technology, Seoul 02792, Republic of Korea, and also with the Department of AI-Robotics, the University of Science and Technology (UST)-KIST School, Seoul 02792, Republic of Korea (e-mail: swkim16@kist.re.kr).

Color versions of one or more figures in this article are available at https://doi.org/10.1109/TMECH.2024.3509854.

Digital Object Identifier 10.1109/TMECH.2024.3509854

I. Introduction

In RECENT years, wearable robots have gained attention as a promising technology for enhancing human functions and capabilities [1], [2], [3]. In the early stage, research focused on developing exoskeletons featuring motorized components and rigid linkages [4], [5]. However, the necessity for users to wear these robots has spurred numerous efforts to enhance wearability, encompassing aspects, such as comfort and overall user experience. This has led to the development of soft wearable robots, which replace traditional rigid linkages with flexible fabrics, resulting in a lighter structure and reduced bulkiness [6], [7]. In addition, robots utilizing force transmission elements, such as wires have been designed to place the actuators in proximal locations instead of directly on human joints [8]. Despite these advancements, the actuator and battery components still occupy a considerable portion of the system, presenting a tradeoff between size/weight reduction and system performance.

Passive wearable robots offer an alternative approach to human augmentation by utilizing nonmotorized mechanical components, such as springs and dampers [9], [10], [11], [12]. Compared with active wearable robots, passive systems are generally lightweight and energy-efficient, as they do not require batteries or actuators, resulting in less maintenance. However, passive wearable robots have limited ability to adapt to varying situations or different users and are constrained in their ability to assist with specific tasks. To address these limitations and enhance versatility in human augmentation solutions, it is essential to be able to adjust the assistance to individuals through the use of sensors and control algorithms [13], [14], [15].

To address the challenges faced in designing wearable robots, quasi-passive wearable robots have been proposed as a hybrid approach [16], [17], [18], [19], [20], [21]. These robots utilize variable springs and dampers capable of mechanical impedance adjustment to change the assistive torque depending on the situation [22]. Alternatively, by utilizing a clutch to control the timing of the mechanical elements' engagement with the user's movement, assistance can be provided only during specific segments of the movement, thereby improving the robot's efficiency and the user's comfort. These approaches offer a solution that is as lightweight and compact as a passive system while providing

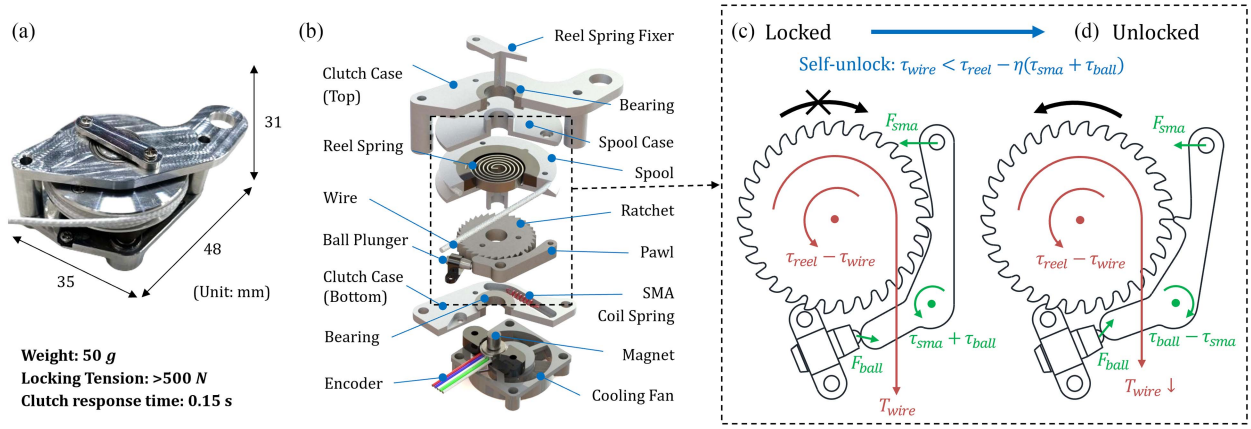

Fig. 1. (a) Configuration of the SuAC and its specification. (b) Exploited view of the clutch and its components. (c) Pawl is fully engaged with the ratchet at the initial state. (d) Pawl is in partial contact with the ratchet at the critical state.

optimized assistance in various situations, such as an active system [15].

Various active clutches with different actuation methods have been used in existing quasi-passive wearable robots. These include electrostatic adhesion [17], servo motors [19], push–pull solenoids [20], and artificial muscles [23]. These compact actuators can drive the clutch with a small power input, providing relatively larger assistive forces, and have been successfully implemented in various applications. However, existing active clutches have the limitation of needing to actively control both locking and unlocking depending on the timing of assistance required. In particular, to ensure the clutch operates effectively in repetitive situations, extensive sensors and advanced control systems are needed to understand the user's intent. This complicates the design, increases cost and maintenance requirements, and can hinder widespread adoption and ease of use.

In this article, we propose a self-unlocking active clutch (SuAC) for use in various quasi-passive wearable robots with reduced actuators, sensors, and control (see Fig. 1 and Supplementary Movie S1). The self-unlocking feature is achieved by mechanically programming the user's intention within their movement. Specifically, the SuAC is designed to unlock autonomously when the assistive force falls below a certain threshold level. This eliminates the need for an additional mechanical triggering component and an external sensor for disengagement, thereby simplifying the design. A shape memory alloy (SMA) coil spring actuator was used as a triggering element for active engagement. The encoder embedded within the SuAC can measure the spool rotation to determine the activation timing.

The rest of this article is organized as follows. Section II describes the design and working principle of the SuAC. Section III provides the design considerations for the SuAC through modeling. Section IV explains the fabrication method and design selection of each component based on the modeling. Section V presents the experimental results on the characteristics of each component and the SuAC as a whole. Section VI demonstrates a device that assists neck movement as an example of a quasi-passive wearable robot utilizing the SuAC's functionality. Finally, Section VII concludes this article.

II. Design

The proposed SuAC is shown in Fig. 1(a) and (b). The spool wound with wire is connected to the top and bottom cases of the clutch through bearings, enabling rotation. Inside the spool, a reel spring is installed, and the central part of this reel spring is fixed to the upper case of the clutch. This allows energy storage in the reel spring when the wire is pulled. The lower part of the spool is fixed with a ratchet, which restricts rotation in the direction of wire pulling depending on the engagement with the pawl. The pawl is affixed to the lower part of the clutch case through the bearing. One end of the pawl contacts a ball plunger, whereas the other connects to an SMA coil spring. The ball plunger contains a preloaded compression spring that exerts a pushing force, providing bistability to the pawl between locking and unlocking states. The SMA coil spring is contracted by electric current and rotates the pawl toward the ratchet engaging the gear teeth. An encoder attached to the clutch's lower case tracks the rotation of the magnet attached to the spool, measuring changes in wire length. A small fan attached to the bottom of the clutch facilitates rapid cooling of the SMA coil spring.

The locking and unlocking of the SuAC are determined by the torque balance of the key components: the ratchet, pawl, ball plunger, SMA coil spring, and reel spring. Fig. 1(c) shows the locking state where the ratchet and pawl are engaged due to the torque τ_{sma} from the SMA. In this case, the torque τ_{ball} from the ball plunger pushes the pawl toward the ratchet, maintaining the locking state. Here, three torque components act on the ratchet. The first component is the torque τ_{wire} from the wire tension. Since the spool cannot rotate in the clockwise direction, the wire tension can increase, and this torque acts on the ratchet in the clockwise direction. The second component is the torque τ_{reel} from the reel spring. The restoring energy stored in the reel spring due to its deflection acts on the ratchet through the spool in the counterclockwise direction. The last component

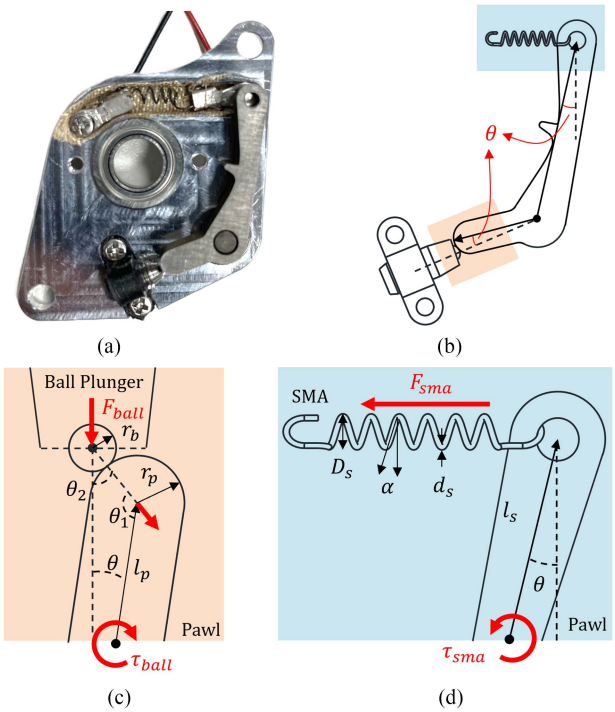

Fig. 2. (a) Internal configuration among the pawl, ball plunger, and SMA coil spring. (b) Schematic of the internal configuration. (c) Scaled view between the pawl and ball plunger with its free body diagram. (d) Scaled view between the pawl and SMA coil spring with its free body diagram.

is the torque from the pawl, transmitted to the ratchet through the gear teeth in contact. This torque is the sum of the SMA and ball plunger torque, acting on the ratchet in the clockwise direction with a gear ratio of η. As a result, when τ_{wire} decreases and becomes less than $\tau_{\text{reel}} - \eta(\tau_{\text{sma}} + \tau_{\text{ball}})$, the ratchet can rotate counterclockwise [see Fig. 1(d)]. Thus, the SuAC can self-unlock without additional actuation, and this feature can be mechanically programmed as a tension threshold determined by the design parameters of each component.

III. Modeling

A. Bistable Pawl With Ball Plunger

Fig. 2(a) shows the pawl, ball plunger, and SMA positioned in the bottom case of the clutch. One end of the pawl is connected to the SMA (pawl actuation tip), whereas the other end contacts the ball plunger (pawl bistability tip). As shown in Fig. 2(b), the pawl actuation tip is designed to be perpendicular to the SMA when the pawl bistability tip is aligned with the ball plunger. When the pawl rotates by θ, the kinematic and kinetic relationships between the pawl, ball plunger, and SMA are illustrated in Fig. 2(c) and (d), respectively.

Fig. 2(c) shows a close-up view of the ball plunger and the pawl. The ball of the plunger and the bistability tip of the pawl are in contact, so the displacement x of the ball plunger is coupled with the rotation angle θ of the pawl. The relationship between x and θ is expressed as follows:

$$\cos\theta = \frac{(l_p + r_p + r_b - x)^2 + l_p^2 - (r_p + r_b)^2}{2l_p(l_p + r_p + r_b - x)} \tag{1}$$

where l_p and r_p are the contact length and radius of the pawl with the ball plunger, respectively. r_b is the radius of the ball plunger. By solving the (1), we can get displacement x as a function of θ. Consequently, the pushing force of the ball plunger is as follows:

$$F_{\text{ball}} = k(s - x) + F_0 \tag{2}$$

where k is the stiffness, s is the maximum stroke, and F_0 is the initial force.

The effective moment arm and force also change according to the pawl's angle θ. The relationships between the variables θ_1, θ_2, and θ are expressed as follows:

$$\frac{r_p + r_b}{\sin\theta} = \frac{l_p + r_p + r_b - x}{\sin\theta_1} \tag{3}$$

$$\frac{r_p + r_b}{\sin\theta} = \frac{l_p}{\sin\theta_2}. \tag{4}$$

By solving the (3) and (4), we can get angles θ_1 and θ_2 as functions of θ. Given these conditions, the torque exerted on the center of rotation of the pawl τ_{ball} can be calculated as follows:

$$\tau_{\text{ball}} = l_p F_{\text{ball}} \cos\theta_2 \sin(\pi - \theta_1). \tag{5}$$

The torque from the ball plunger pushes the pawl toward and away from the ratchet for locking and unlocking without continuous actuation. This can be characterized by the pawl's snap-through torque to overcome the bistability between the locked and unlocked states.

B. Active Locking With SMA Coil Spring

A compact and lightweight trigger element is sufficient to actively engage the pawl to the ratchet by overcoming the bistability. Various actuation methods have been employed as triggers in previous wearable robots, including solenoid actuators [24], pneumatic actuators, and SMA actuators [23]. Among these, the SMA actuator features a high power density with respect to its weight and size. Thus, we selected the SMA coil spring as a triggering actuator to engage the pawl.

Based on previous studies of the design of SMA coil spring [25], [26], we can design the SMA coil spring satisfying the requirements of the proposed clutch. The actuation characteristics of SMA coil springs, especially force and displacement, can be defined by several design factors with geometric configurations and material properties. Specifically, as shown in Fig. 2(d), d is the wire diameter, D is the coil diameter, n is the number of coils, and α is the pitch angle. Concurrently, the material properties include the shear modulus G and Poisson's ratio ν.

The displacement of the SMA coil spring, denoted as δ, can be defined as follows:

$$\delta = \frac{\pi N_s D_s}{\cos\alpha_i}(\sin\alpha_f - \sin\alpha_i) \tag{6}$$

where the subscriptions indicate that i and f are initial and final states, respectively.

The actuation force of the SMA coil spring can be calculated as (7) for the 100% austenite state and (8) for the 100% martensite state at a low temperature

$$F_A = \frac{G_A d_s^4}{8D_s^3 N_s}\frac{\cos^3\alpha_{Ai}}{K_{Af}}\delta \tag{7}$$

$$F_M = \frac{G_M d_s^4}{8D_s^3 N_s}\frac{\cos^3\alpha_{Mi}}{K_{Mf}}\delta - \frac{\pi d_s^3}{8D_s}G_M\gamma_L\xi_{S\gamma} \tag{8}$$

where $K_x = \cos^2\alpha_x(\cos^2\alpha_x + \sin^2\alpha_x/(1+\nu))$, with x representing either Af or Mf for each phase state of the SMA coil spring. The subscriptions A and M indicate austenite and martensite states, respectively. γ_L is the residual strain, and $\xi_{S\gamma}$ is the detwinned martensite volume fraction of the SMA coil spring.

The shear strain, γ, can be calculated as follows:

$$\gamma = \frac{d_s}{D_s}\frac{\cos^2\alpha_i(\sin\alpha_f - \sin\alpha_i)}{K_f}. \tag{9}$$

The detwinned martensite volume fraction, $\xi_{S\gamma}$, can be calculated as follows:

$$\xi_{S\gamma} = \frac{1}{2}\cos\left(\frac{\pi}{\gamma_s^{cr} - \gamma_f^{cr}}(\gamma - \gamma_f^{\mathrm{cr}})\right) + \frac{1}{2} \tag{10}$$

where γ_S^{cr} is the critical strain for detwinning start and γ_f^{cr} is the critical strain for detwinning finish.

The shear modulus G, residual strain γ_L, and critical strains for detwinning start γ_S^{cr} and finish γ_f^{cr} should be obtained from the tensile experiment of the SMA spring

$$\tau_{\mathrm{sma}} = l_s F_{\mathrm{sma}}\cos\theta \tag{11}$$

where l_s is the pawl's actuation tip length.

To successfully engage the pawl with the ratchet, the torque generated by the tension of the SMA coil spring must be higher than the snap-through torque to overcome the bistability of the pawl. Therefore, the specific conditions for the SMA coil spring to successfully lock the clutch are as follows:

$$\text{Locking:}\quad \tau_{\mathrm{sma}} > \tau_{\mathrm{ball}}. \tag{12}$$

C. Energy Storage With Reel Spring

In this work, we utilized a reel spring as the energy storage element within the SuAC due to its compactness and large deflection capacity. As shown in Fig. 3(a), the reel spring is integrated within the spool. With the core of the reel spring fixed to the clutch case and the outer end fixed to the spool, pulling the wire rotates the spool and stores energy within the reel spring. The torque of the reel spring τ_{reel} can be represented as follows:

$$\tau_{\mathrm{reel}} = \frac{Ebt^3}{6\pi N_r(D_r + d_r)}\phi \tag{13}$$

where ϕ is the deflection angle, b is the material width, t is the material thickness, N_r is the number of turns, D_r is the outer diameter, d_r is the inner diameter, and E is the elastic modulus, as depicted in Fig. 3(b).

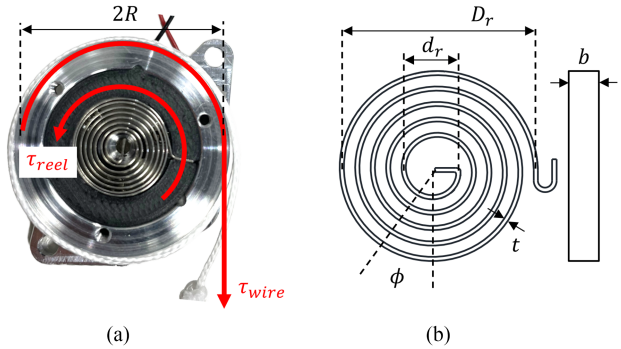

Fig. 3. (a) Internal configuration of the spool with the reel spring. (b) Geometric parameters of reel spring (top and side views).

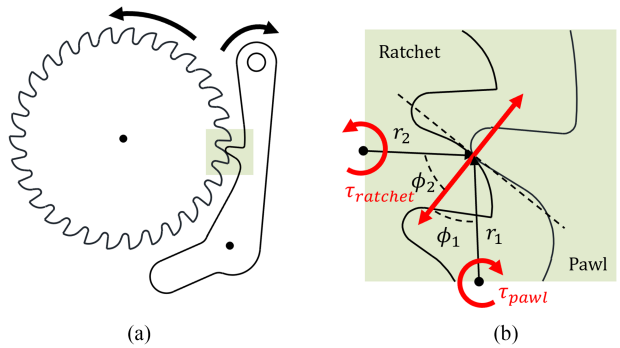

Fig. 4. (a) Ratchet rotates counterclockwise, and the pawl rotates clockwise during the transition from the locking state to the unlocking state. (b) Scaled view between the ratchet and pawl with its free-body diagram.

The torque of the reel spring increases in proportion to the angular deflection ϕ, and its slope is determined by the spring's stiffness, which is set by the design parameters. The reel spring's torque plays two key roles depending on the state of the clutch.

The first role is in the unlocked state, where the torque from the reel spring is transferred through the spool to the wire tension, preventing slack in the wire and allowing it to naturally follow the user's movements. The wire tension can be expressed as $T_{\mathrm{wire}} = \tau_{\mathrm{reel}}/R$, where R is the radius of the spool. If the reel spring torque is too large, it may create unnecessary resistance even when user assistance is not needed, potentially hindering the user's motion.

The second role is in the locked state, where the torque from the reel spring acts as a force that drives the ratchet against the pawl. Therefore, an appropriate amount of reel spring torque is essential for the self-unlocking of the clutch. Details for this self-unlocking condition are discussed in the next section.

D. Self-Unlocking Condition

As shown in Fig. 4(a), the ratchet can rotate in the direction that pushes out the pawl. The traveling angle of the pawl, from the initial locking state where the pawl is fully engaged with the ratchet to the critical state where the teeth are in partial contact,

TABLE I
COMPARISON OF DIFFERENT STUDIES

Study	Locking	Unlocking	Clutch weight	Locking tension	Dimension
Diller et al. [17]	Active	Active	26 g	501 N	2.5 x 100 x 300 mm
Chang et al. [19]	Active	Active	442 g	90 N	700 x 900 x 900 mm **
Wang et al. [20]	Active	Active	104 g	138 N *	20 x 43 x 56 mm
Park et al. [23]	Active	Active	83 g	75 N	20 x 40 x 40 mm **
This study	**Active**	**Passive**	**50 g**	**542 N**	**31 x 35 x 48 mm**

Locking tension refers to the maximum force tested in the article.
* Calculated using assistive torque, ** Estimated from the provided figure.

is calculated as follows:

$$\Delta\theta = \arctan\left(\frac{d_{r,o}}{d_p}\right) - \arccos\left(\frac{d_p^2 + d^2 - d_{r,i}^2}{2d_p d}\right) \quad (14)$$

where $d_{r,i}$ and $d_{r,o}$ are the inner and outer radius of the ratchet's tooth, respectively, and d_p is the radius of the pawl's tooth. For simplicity, when the ratchet and pawl make partial contact with their single teeth, they are arranged such that the contact point forms a right angle from their respective centers of rotation $d = \sqrt{d_{r,o}^2 + d_p^2}$.

In this process, the torque transfer between the ratchet and pawl is given by the relationship $\tau_{\text{ratchet}} = \eta\tau_{\text{pawl}}$ [see Fig. 4(b)]. Here, the gear ratio η is defined as follows:

$$\eta = \frac{r_2 \sin\phi_2}{r_1 \sin\phi_1} \quad (15)$$

where r_1 and r_2 are the radius, and and ϕ_1 and ϕ_2 are the pressure angle of the pawl and ratchet at the contact point, respectively.

The torque acting on the ratchet is the difference between the torque provided by the reel spring and the torque due to the wire, $\tau_{\text{ratchet}} = \tau_{\text{reel}} - \tau_{\text{wire}}$. The ratchet rotates counterclockwise to overcome the bistability of the pawl when the ratchet torque exceeds the torque provided by the pawl, $\tau_{\text{ratchet}} > \eta\tau_{\text{pawl}}$. At this time, the torque acting on the pawl is the sum of the torque provided by the SMA and the torque provided by the ball plunger, $\tau_{\text{pawl}} = \tau_{\text{sma}} + \tau_{\text{ball}}$. Consequently, the condition for the ratchet to rotate counterclockwise and push out the pawl for self-unlocking can be expressed as follows:

$$\text{Self-unlocking:} \quad \tau_{\text{wire}} < \tau_{\text{reel}} - \eta(\tau_{\text{sma}} + \tau_{\text{ball}}). \quad (16)$$

IV. FABRICATION

In this section, we describe the fabrication process of the SuAC based on the modeling considerations explained in Section III. First, we considered the clutch's maximum locking torque, which is directly related to the maximum assistance force. This value can vary depending on the application, we set the maximum locking tension to 500 N, which is generally not exceeded in wire-driven wearable robots. Given the spool radius of R = 14 mm used in this study, and the corresponding locking torque is 7 Nm.

To withstand this locking torque, the dimensions of the ratchet and pawl were determined through FEA simulations using Solidworks (Dassault Systèmes) [see Fig. 5(a)]. In the simulations, most of the dimensions of the ratchet and pawl were fixed based on the previously analyzed model, and the thickness was varied to verify whether the components could withstand the required torque. The material property was plane carbon steel with Young's modulus of approximately 210 GPa. Concentrated loads were applied to the contact surface between the ratchet and pawl to ensure the material did not yield under maximum stress, and the minimum thickness was selected to maintain a safety factor of 1.5. The selected parameters for the ratchet and pawl are detailed in Table II.

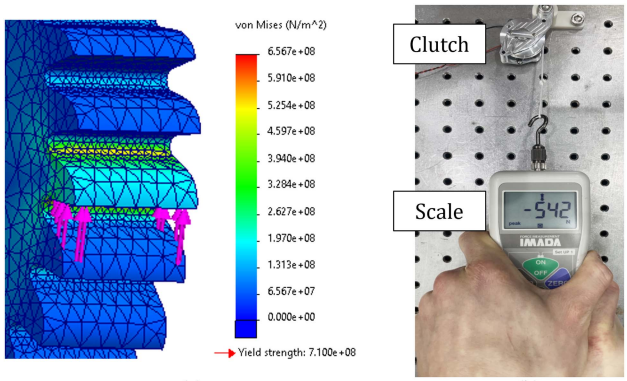

Fig. 5. (a) Stress distribution on ratchet teeth from FEA. (b) Allowable locking tension of 542 N (video is available in Supplementary Movie S2).

TABLE II
SPECIFICATION OF RATCHET AND PAWL

Specification	Symbol [unit]	Value
Thickness	t [mm]	4
Ratchet tooth number	N_t [number]	30
Ratchet tooth inner distance	$d_{r,i}$ [mm]	8.6
Ratchet tooth outer distance	$d_{r,o}$ [mm]	10
Ratchet tooth radius	c_r [mm]	1.2
Pawl tooth distance	d_p [mm]	9
Pawl tooth radius	c_p [mm]	0.3
Pawl bistability tip length	l_p [mm]	6.5
Pawl bistability tip radius	r_p [mm]	1.5
Pawl actuation tip length	l_s [mm]	16

Based on (14), the traveling angle $\Delta\theta$ of the pawl from the initial locking state to the critical state is calculated to be 8.95°. When the pawl rotates by half of this angle, the ball plunger is aligned parallel to the pawl's bistability tip. In this study, we used a ball plunger with a stroke length of 0.5 mm, a ball radius of 0.75 mm, and a stiffness of 5.6 N/mm (Misumi, South Korea), and

TABLE III
SPECIFICATION OF SMA COIL SPRING

Specification	Symbol [unit]	Value
Wire diameter	d_s [mm]	0.254
Coil diameter	D_s [mm]	1.5
Number of coils	N_s [number]	5
Initial pitch angle	α_i [rad]	0.053

TABLE IV
SPECIFICATION OF REEL SPRING

Specification	Symbol [unit]	Value
Material width	b [mm]	3
Material thickness	t [mm]	0.3
Number of coils	N_r [number]	6.5
Outer diameter	D_r [mm]	14.5
Inner diameter	d_r [mm]	3

τ_{ball} was calculated to be 15.67 Nm based on (5) (see Section V for the specific characteristics of the ball plunger).

Subsequently, the SMA coil spring was designed to meet (12). The required tension when the SMA coil spring is in the austenite phase is 0.98 N. In addition, to overcome the bistability during actuation, the pawl needs to rotate by $\Delta\theta/2$, which is 4.48°. Therefore, the minimum displacement required for the SMA coil spring to contract is calculated as $\Delta\delta = l_s\Delta\theta/2$, which is 1.25 mm. The geometric specifications of the selected SMA coil spring are provided in Table III.

When the clutch is unlocked, the reel spring stores energy and maintains tension proportional to the wire's displacement. The high stiffness of the reel spring when the wearable robot's assistance is not needed can unnecessarily resist the user's movement. Conversely, if the reel spring's stiffness is too low, there will be insufficient torque for self-unlocking in the clutch's locked state. It may also hinder wire retraction due to the rotational friction within the clutch. To meet these upper and lower boundary conditions, we used a reel spring with a stiffness of 6.8 Nmm/rad by preloading an initial torque of 30 Nmm (Springfarm, Republic of Korea). The design parameters of the reel spring are given in Table IV.

The top and bottom cases and the spool of the clutch were manufactured from A7075-T6 aluminum alloy. The ratchet and pawl were fabricated from medium carbon chromium molybdenum alloy steel SCM440, using wire electrical discharge machining. Other components, including the reel spring holders, ball plunger, and encoder housing, were 3-D printed (X7, MarkForged Inc., USA). The SMA coil spring was fabricated following the method described in previous research [27]. A commercial nickel–titanium alloy wire (Flexinol, Dynalloy Inc., USA) was coiled around a stainless steel rod, heat-treated at 400°C for an hour, and then naturally cooled. The fabricated SMA coil spring was attached to one end of the pawl using a plastic M2 bolt to prevent electrical current flow. To ensure electrical insulation from the clutch casing during operation and to reduce friction, the slot housing the SMA coil spring was lined with heat-resistant PTFE-coated glass tape (Taconic, South Korea). A small incremental encoder (RM08, RLS, Slovenia) was mounted on the lower clutch case to monitor the displacement and direction of the wire. Finally, a small fan (MS2507, Mechatronics, USA) was attached for the rapid cooling of the SMA coil spring.

Consequently, the resulting SuAC, depicted in Fig. 1(a), has a lightweight design with a mass of 50.3 g and compact overall dimensions of 31 mm in height, 35 mm in width, and 48 mm in depth. In addition, using a digital force measurement gauge (DS2-1000N, Imada, USA), we confirmed that the clutch could reliably withstand forces exceeding 542 N and achieve self-unlocking [see Fig. 5(b) and Supplementary Movie S2].

TABLE V
SPECIFICATION OF BALL PLUNGER

Specification	Symbol [unit]	BMS	BSM	BSZF	BSX
Stroke	s [mm]	0.5			
Ball radius	r_b [mm]	0.75			
Initial force	F_0 [N]	0.3	1.0	1.5	2.2
Stiffness	k [N/mm]	0.7	2.0	3.0	5.6

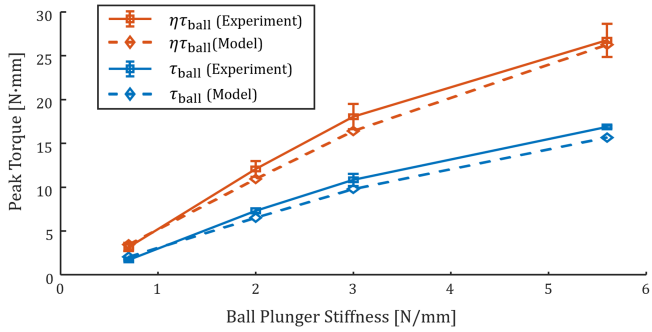

Fig. 6. Comparison of bistability snap-through torque over ball plunger stiffness for pawl and ratchet, between experimental results and model predictions.

V. EXPERIMENTAL RESULTS

A. Bistability Snap-Through Torque

We measured the snap-through torque τ_{ball} required to overcome the bistability provided by the ball plunger to the pawl. To simplify the experiment, we attached a wire to the pawl instead of using an SMA coil spring and measured the force when the wire was pulled very slowly. Subsequently, we measured the snap-through torque of the pawl using the ratchet mechanism. We wound the wire around a spool connected to the ratchet and measured the force generated as the wire was pulled slowly. The snap-through torque of the pawl was calculated by multiplying the peak force by the pawl's moment arm $l_s = 16$ mm. The snap-through torque of the ratchet was determined by multiplying the peak force by the spool radius $R = 14$ mm. The experiment utilized four commercially available ball plungers, with detailed specifications provided in Table V. Each experiment was repeated five times for each ball plunger, and the maximum force observed in each case was used for analysis.

The snap-through torque values corresponding to the stiffness of the ball plungers are shown in Fig. 6. The experimental

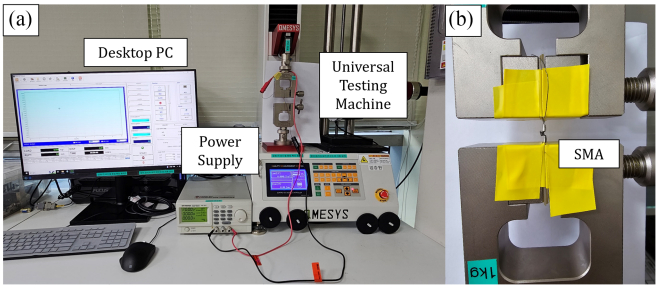

Fig. 7. Experiment setup for SMA coil spring characterization. (a) Overall experiment setup. (b) Clamped SMA coil spring with electric insulation.

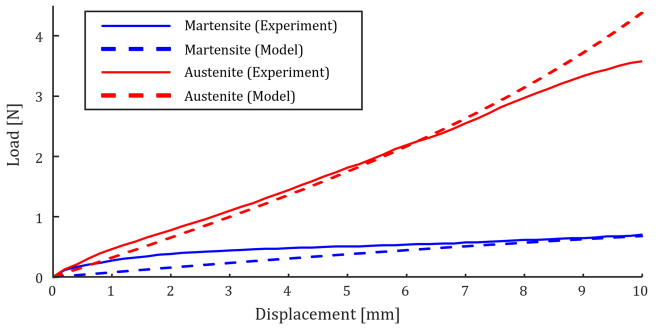

Fig. 8. Comparison of the load versus displacement for both Martensite and Austenite phases, between experimental results and model predictions.

values, represented by error bars, indicate the mean and standard deviation. The results demonstrate that as the stiffness of the ball plungers increases, the energy barrier of bistability also increases, leading to higher snap-through torque values. The experimental data for the snap-through torque of the ratchet showed a more significant variance compared with that of the pawl due to the frictional forces between the ratchet and the pawl. We compared these results with the snap-through torque values modeled based on the specifications of the ratchet and pawl determined in Section IV and the modeling described in Section III. The gear ratio between the ratchet and pawl η was calculated from (15) and set to 1.68. The modeling predictions aligned well with the experimental values, validating that it is feasible to predict the snap-through torque based on the design specifications of the ratchet, pawl, and ball plungers.

B. SMA Coil Spring Characterization

The characteristics of the SMA coil spring were measured using a universal testing machine (QMESYS, South Korea), as shown in Fig. 7. First, the tensile force of the SMA coil spring in both martensite and austenite states was measured according to displacement. As shown in Fig. 8, the experimental results were compared with the predicted values based on modeling. The material properties used in the modeling included Poisson's ratio provided in the manufacturer's datasheet, and the shear modulus, residual strain, and critical strain values for the start and end of twinning obtained through experimentation.

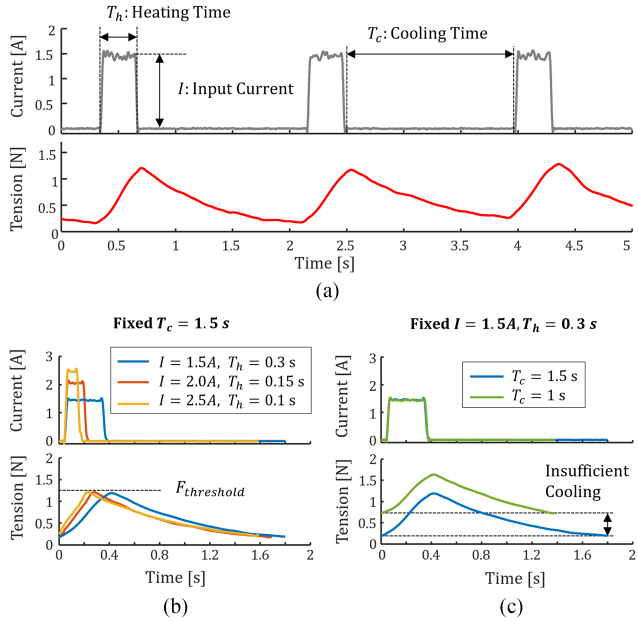

Fig. 9. Cyclic characteristics of SMA coil spring. (a) Impact of electric currents on phase transition through Joule heating is visible in tension variation. (b) Heating time needed for austenite phase transition at various currents. (c) Cooling time needed for martensite phase transition.

The experimental results closely matched the model predictions, considering the slight discrepancy due to the asymmetry at both ends of the SMA coil spring. The displacement at which the SMA coil spring in the austenite state generates a force of 1 N to overcome the snap-through torque by the ball plunger is 2.5 mm. Therefore, considering the contraction length of the SMA coil spring, it was confirmed that when the initial length is set to at least 3.75 mm, the pawl can be reliably engaged with the ratchet.

We also explored the cyclic characteristics of the SMA coil spring that affect the clutch's operating frequency. Joule heating from electrical current activates the SMA coil spring, impacting the austenite-martensite phase transition based on the current magnitude and heating/cooling durations [see Fig. 9(a)]. We applied varying currents to a 4 mm fixed SMA coil spring, measuring the time to generate a force over 1.2 N under different heating and cooling times. During the experiment, we applied convective cooling through the fan used in the clutch. We first explored the required heating time with fixed cooling time and then explored the required cooling time with fixed heating time. For each condition, the heating and cooling of the SMA coil spring were repeated five times consecutively.

Fig. 9(b) and (c) shows the mean values of input current and tension over the repeated cycles. As shown in Fig. 9(b), Joule heating with 1.5, 2, and 2.5 A required approximately 0.3, 0.15, and 0.1 s, respectively, to achieve 1.2 N. This indicates that the required heating time is nonlinearly reverse-proportional to the current magnitude. Fig. 9(c) shows the changes in tension when cooling times of 1 and 1.5 s were applied after reaching 1.2 N. When the cooling time was 1.5 s, the tension change converged to 0.4 N, whereas with 1 s, it resulted in overall upward shifting

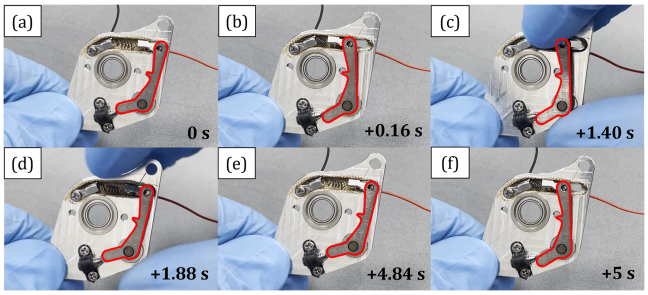

Fig. 10. Sequential time snapshots of the active engagement process by the SMA coil spring (Video is available in Movie S3). (a) Initial unlocking state (before trigger). (b) Locking state (after the momentary trigger). (c) Manual unlocking. (d) Maintained in the unlocking state due to the bistability. (e) Unlocking state (before trigger). (f) Locking state (after the momentary trigger).

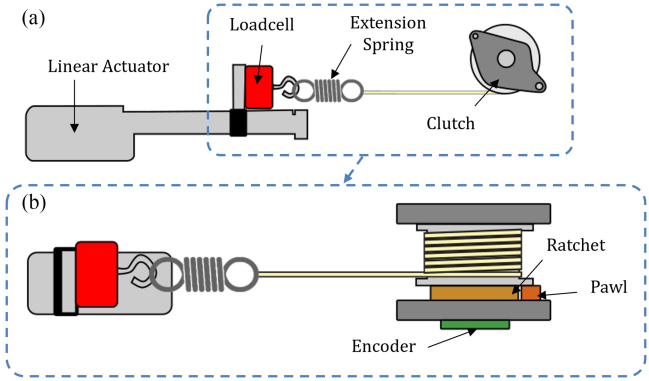

Fig. 11. Schematic of the experimental setup, including the clutch, extension spring, linear actuator, and loadcell. (a) Top view. (b) Side view.

due to overheating. This indicates that a minimum cooling time of 1.5 s is required for a complete phase transition from austenite to martensite. Rapid actuation without sufficient cooling could cause permanent deformation of the SMA coil spring, altering its actuation characteristics. Therefore, for stable repetitive use of the clutch, it is recommended to apply Joule heating for 0.1 s at 2.5 A, followed by cooling for 1.5 s. The calculated cycle time is 1.6 s, resulting in an actuation frequency of approximately 0.625 Hz.

In the sequence shown in Fig. 10, the active engagement mechanism of the SMA coil spring is demonstrated (Supplementary Movie S3). Initially, the clutch is unlocked with the spring relaxed at ambient temperature, indicating a martensite phase [see Fig. 10(a)]. Upon receiving a current pulse, the SMA undergoes a rapid phase transition to austenite, resulting in the spring's retraction and subsequent clutch engagement into a locked state [see Fig. 10(b)]. The process of manual unlocking is then depicted, where an external force is applied to return the spring to its original shape [see Fig. 10(c)]. After manual unlocking, the clutch remains unlocked due to its bistability, eliminating the need for continuous external energy [see Fig. 10(d)]. The sequence concludes by showing the clutch's capability for repeatable actuation [see Fig. 10(e) and (f)].

C. Clutch Evaluation

We conducted an experiment to evaluate our proposed clutch, focusing on its response time over the cyclic activation. As shown in Fig. 11, the experimental setup includes a clutch, an extension spring, a linear actuator, and a load cell. A load cell (LSB205, Futek, USA) is attached to the end of a linear actuator (T16, Actuonix, Canada) to measure the tension in the wire, which varies with the displacement. An extension spring is connected in series to the wire from the clutch, which changes the tension profile depending on the locking state of the clutch. A custom controller utilizing an STM32F4 microcontroller (STMicroelectronics, Switzerland) measures the displacement of the wire via the encoder and controls the actuation timing of the clutch. In addition, this controller operates with the linear actuator driver (LAC, Actuonix, Canada) and amplifier (IAA100, Futek, USA) to control the actuator and measure tension during the clutch engagement and release phases.

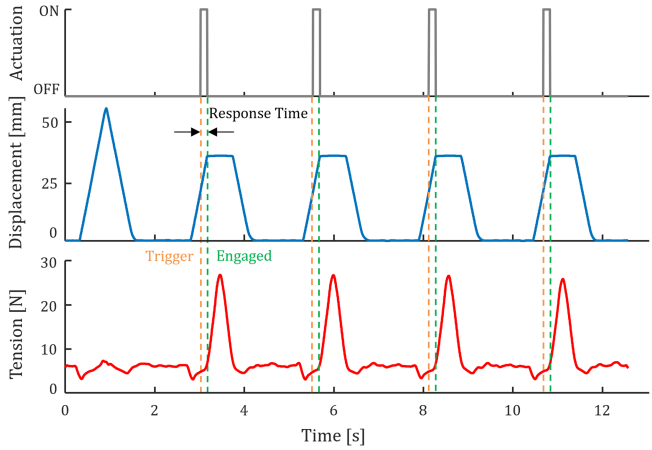

Fig. 12. Experimental results over time. The binary actuation state of an SMA coil spring (top), the clutch spool angle (middle), and the wire tension (bottom).

Fig. 12 shows the activation of the clutch, variations in clutch spool angle, and wire tension over time. The linear actuator simulates the user's movement and is programmed to move back and forth. During the initial cycle, the clutch remains inactive, whereas it is activated in the subsequent four cycles. The tension shows two distinct profiles depending on the clutch state due to the serially connected internal reel spring and external extension spring. When the clutch is unlocked, the tension of the relatively less stiff reel spring is measured. In contrast, when the clutch is locked, the reel spring is fixed in place, measuring the tension of the extension spring.

The orange dashed vertical line indicates the moment of clutch actuation programmed at the wire displacement of 35 mm. The green dashed vertical line indicates when the clutch's spool angle becomes stationary after the engagement of the pawl with the ratchet. Over the 50 cycles, we collected the time interval between the orange and green lines and observed the response time (0.15 ± 0.02 s). The results demonstrate the clutch's

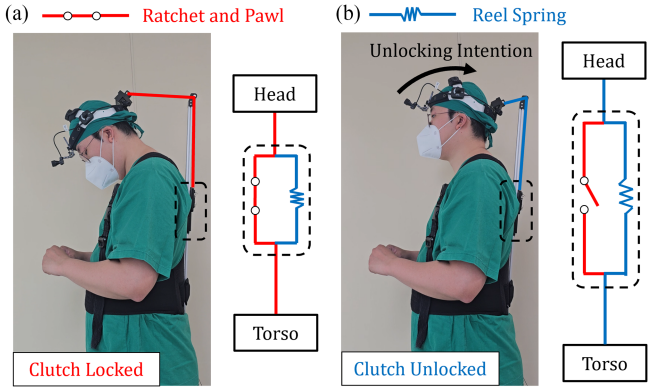

Fig. 13. Operation of the neck support exosuit. (a) When the clutch is locked, the head and torso are connected, supporting the neck muscles during head flexion. (b) When the clutch unlocks, the user can freely move their head. (Video is available in Supplementary Movie S4).

ability to provide assistance rapidly, and once it starts assisting, no further energy is consumed. Moreover, the self-unlocking feature can utilize the single encoder data embedded within the clutch, ensuring robust and consistent actuation.

VI. Application

We demonstrate a neck support exosuit as an example of how SuAC can be applied to various quasi-passive wearable robots (Supplementary Movie S4). Prolonged neck flexion during surgical procedures can cause neck pain [28]. In addition, surgeons need to use both hands during the surgery, requiring sensors and complex algorithms to read the user's intent for controlling the exosuit's support. There has been a study on passive neck support exosuit [29], they have the limitation of hindering free movement due to the displacement-proportional assistive force that is constantly applied, even when assistance is not needed. Therefore, by applying SuAC to the neck support exosuit, we demonstrate that it can provide simple yet effective neck support without additional sensors or complex control algorithms.

The developed neck support exosuit consists of a headgear and a vest, each having anchoring points on the head and torso. On the back of the vest, a strut extends vertically from the user's torso to the back of the head, and a clutch is attached. The clutch wire passes through a pulley attached to the end of the strut and is connected to the back of the headgear. When the clutch is locked [see Fig. 13(a)], the head and torso are connected by the wire, supporting the neck extensor muscles when the user bends their head. In addition, when the user tilts his head back, the clutch automatically unlocks [see Fig. 13(b)], allowing the user to move their head freely without interference from the exosuit. This provides a simple yet functional device controlled solely by the user's movements without additional sensors. The effectiveness of this device in reducing neck muscle fatigue will be verified through further studies.

VII. Conclusion and Discussion

In this study, we proposed a SuAC that automatically unlocks in response to the user's movements. This design leverages a unique combination of mechanical intelligence and simplicity without the need for external sensors or additional mechanical triggers. Through comprehensive analysis, we established detailed design guidelines outlining the kinematic and dynamic conditions necessary for effectively designing the clutch components. Based on these guidelines, we developed a proof-of-concept clutch that weighs approximately 50 g, can actively lock the wire within 0.15 s, and withstands forces exceeding 500 N. By applying SuAC to the neck support exosuit, we demonstrated an energy-efficient and low-complexity system that maximizes the self-unlocking feature based on the user's movements. We believe these research findings highlight SuAC's adaptability and potential to enhance the overall functionality of various quasi-passive wearable devices.

The potential applications of the SuAC are diverse and can be integrated into various wearable robots designed to augment muscle support and spring functions [30]. For example, in scenarios similar to the neck support device, the SuAC could be applied to shoulder exosuits that assist industrial workers in lifting their arms overhead [8]. In addition, the SuAC could be used in ankle exoskeletons in combination with springs to provide support while standing and not impede movement while walking [17], [20]. However, this study has limitations in scenarios requiring rapid cycling of clutch locking and unlocking. This limitation arises from the relatively low repetition rate due to the cooling time required for the SMA coil spring. To address this, future research should explore existing studies that can reduce the cooling time of SMA coil springs [31], [32] or investigate alternative trigger methods with faster responsiveness. Future studies will focus on optimizing SuAC's performance by integrating advanced materials and technologies, expanding its applicability to support a wide range of human activities, and verifying its effectiveness.

References

[1] J. L. Pons, *Wearable Robots: Biomechatronic Exoskeletons*. Hoboken, NJ, USA: John Wiley and Sons, 2008.
[2] A. Esquenazi, M. Talaty, A. Packel, and M. Saulino, "The rewalk powered exoskeleton to restore ambulatory function to individuals with thoracic-level motor-complete spinal cord injury," *Amer. J. Phys. Med. Rehabil.*, vol. 91, no. 11, pp. 911–921, 2012.
[3] T. Yan, M. Cempini, C. M. Oddo, and N. Vitiello, "Review of assistive strategies in powered lower-limb orthoses and exoskeletons," *Robot. Auton. Syst.*, vol. 64, pp. 120–136, 2015.
[4] A. M. Dollar and H. Herr, "Lower extremity exoskeletons and active orthoses: Challenges and state-of-the-art," *IEEE Trans. Robot.*, vol. 24, no. 1, pp. 144–158, Feb. 2008.
[5] S. Yu et al., "Quasi-direct drive actuation for a lightweight hip exoskeleton with high backdrivability and high bandwidth," *IEEE/ASME Trans. Mechatronics*, vol. 25, no. 4, pp. 1794–1802, Aug. 2020.
[6] A. T. Asbeck, S. M. De Rossi, I. Galiana, Y. Ding, and C. J. Walsh, "Stronger, smarter, softer: Next-generation wearable robots," *IEEE Robot. Automat. Mag.*, vol. 21, no. 4, pp. 22–33, Dec. 2014.
[7] J. Bae et al., "A lightweight and efficient portable soft exosuit for paretic ankle assistance in walking after stroke," in *Proc. IEEE Int. Conf. Robot. Automat.*, 2018, pp. 2820–2827.
[8] S. Ding, F. Anaya-Reyes, A. Narayan, S. Ofori, S. Bhattacharya, and H. Yu, "A lightweight shoulder exoskeleton with a series elastic actuator for assisting overhead work," *IEEE/ASME Trans. Mechatronics*, vol. 29, no. 2, pp. 1030–1040, Apr. 2024.
[9] W. Van Dijk, H. Van Der Kooij, and E. Hekman, "A passive exoskeleton with artificial tendons: Design and experimental evaluation," in *Proc. 2011 IEEE Int. Conf. Rehabil. Robot.*, 2011, pp. 1–6.

[10] S. H. Collins, M. Bruce Wiggin, and G. S. Sawicki, "Reducing the energy cost of human walking using an unpowered exoskeleton," *Nature*, vol. 522, no. 7555, pp. 212–215, 2015.
[11] X. Wang, S. Guo, B. Qu, M. Song, and H. Qu, "Design of a passive gait-based ankle-foot exoskeleton with self-adaptive capability," *Chin. J. Mech. Eng. (English Edition)*, vol. 33, 2020, Art. no. 49.
[12] E. Etenzi, R. Borzuola, and A. M. Grabowski, "Passive-elastic knee-ankle exoskeleton reduces the metabolic cost of walking," *J. NeuroEngineering Rehabil.*, vol. 17, no. 1, pp. 1–15, 2020.
[13] J. Zhang et al., "Human-in-the-loop optimization of exoskeleton assistance during walking," *Science*, vol. 356, no. 6344, pp. 1280–1283, 6 2017.
[14] P. Slade, M. J. Kochenderfer, S. L. Delp, and S. H. Collins, "Personalizing exoskeleton assistance while walking in the real world," *Nature*, vol. 610, no. 7931, pp. 277–282, 2022.
[15] B. A. Shafer, J. C. Powell, A. J. Young, and G. S. Sawicki, "Emulator-based optimization of a semi-active hip exoskeleton concept: Sweeping impedance across walking speeds," *IEEE Trans. Biomed. Eng.*, vol. 70, no. 1, pp. 271–282, Jan. 2023.
[16] K. Shamaei, M. Cenciarini, A. A. Adams, K. N. Gregorczyk, J. M. Schiffman, and A. M. Dollar, "Design and evaluation of a quasi-passive knee exoskeleton for investigation of motor adaptation in lower extremity joints," *IEEE Trans. Biomed. Eng.*, vol. 61, no. 6, pp. 1809–1821, Jun. 2014.
[17] S. Diller, C. Majidi, and S. H. Collins, "A lightweight, low-power electroadhesive clutch and spring for exoskeleton actuation," in *Proc. IEEE Int. Conf. Robot. Automat.*, 2016, pp. 682–689.
[18] S. Kumar, M. R. Zwall, E. A. Bolivar-Nieto, R. D. Gregg, and N. Gans, "Extremum seeking control for stiffness auto-tuning of a Quasi-passive ankle exoskeleton," *IEEE Robot. Automat. Lett.*, vol. 5, no. 3, pp. 4604–4611, Jul. 2020.
[19] Y. Chang, W. Wang, and C. Fu, "A lower limb exoskeleton recycling energy from knee and ankle joints to assist push-off," *J. Mechanisms Robot.*, vol. 12, no. 5, 2020, Art. no. 051011.
[20] C. Wang et al., "Design of an ankle exoskeleton that recycles energy to assist propulsion during human walking," *IEEE Trans. Biomed. Eng.*, vol. 69, no. 3, pp. 1212–1224, Mar. 2022.
[21] L. Miskovic, M. Dezman, and T. Petric, "Pneumatic quasi-passive variable stiffness mechanism for energy storage applications," *IEEE Robot. Automat. Lett.*, vol. 7, no. 2, pp. 1705–1712, Apr. 2022.
[22] B. H. Do, I. Choi, and S. Follmer, "An all-soft variable impedance actuator enabled by embedded layer jamming," *IEEE/ASME Trans. Mechatronics*, vol. 27, no. 6, pp. 5529–5540, Dec. 2022.
[23] S. J. Park, J. Jeong, M. Won, and C. H. Park, "Locking-unlocking mechanism actuated by SMA springs to improve the energy efficiency of fabric-type soft actuators," *Smart Mater. Struct.*, vol. 28, no. 12, 2019, Art. no. 125005.
[24] S. Yin, B. Shi, G. Liu, J. Wang, and C. Zhao, "Electromagnetic clutch-based ankle exosuit for assisting stroke survivors with different body sizes," *IEEE Robot. Automat. Lett.*, vol. 8, no. 8, pp. 4847–4854, Aug. 2023.
[25] S. M. An, J. Ryu, M. Cho, and K. J. Cho, "Engineering design framework for a shape memory alloy coil spring actuator using a static two-state model," *Smart Mater. Struct.*, vol. 21, no. 5, 2012, Art. no. 055009.
[26] J. S. Koh, "Design of shape memory alloy coil spring actuator for improving performance in cyclic actuation," *Mater.*, vol. 11, no. 11, 2018, Art. no. 2324.
[27] S. W. Kim, J. G. Lee, S. An, M. Cho, and K. J. Cho, "A large-stroke shape memory alloy spring actuator using double-coil configuration," *Smart Mater. Struct.*, vol. 24, no. 9, 2015, Art. no. 95014.
[28] K. Welcker, E. B. Kesieme, E. Internullo, and L. J. Kranenburg Van Koppen, "Ergonomics in thoracoscopic surgery: Results of a survey among thoracic surgeons," *Interactive Cardiovasc. Thoracic Surg.*, vol. 15, no. 2, pp. 197–200, 2012.
[29] E. Tetteh, M. S. Hallbeck, and G. A. Mirka, "Effects of passive exoskeleton support on EMG measures of the neck, shoulder and trunk muscles while holding simulated surgical postures and performing a simulated surgical procedure," *Appl. Ergonom.*, vol. 100, 2022, Art. no. 103646.
[30] M. H. Dickinson, C. T. Farley, R. J. Full, M. A. Koehl, R. Kram, and S. Lehman, "How animals move: An integrative view," *Science*, vol. 288, no. 5463, pp. 100–106, 2000.
[31] A. Lara-Quintanilla and H. E. Bersee, "Active cooling and strain-ratios to increase the actuation frequency of SMA wires," *Shape Memory Superelasticity*, vol. 1, no. 4, pp. 460–467, 2015.
[32] Q. Ding, J. Chen, W. Yan, K. Yan, A. Kyme, and S. S. Cheng, "A high-performance modular SMA actuator with fast heating and active cooling for medical robotics," *IEEE/ASME Trans. Mechatron.*, vol. 27, no. 6, pp. 5902–5913, Dec. 2022.

Jae-Ryeong Choi (Graduate Student Member, IEEE) received the B.S. degree in mechanical engineering from the Pohang University of Science and Technology, Pohang, Republic of Korea, in 2018. He is currently working toward the Ph.D. degree in mechanical engineering with the BioRobotics Laboratory, Seoul National University, Seoul, Republic of Korea.

His research interests include wearable devices, novel mechanism designs, and rehabilitation/assistive robotics.

Seung-Won Kim (Member, IEEE) received the B.S. and Ph.D. degrees in mechanical and aerospace engineering from Seoul National University, Seoul, Republic of Korea, in 2009 and 2016, respectively.

He was a research scientist from 2016 to 2018, and a senior research scientist from 2018 to 2024, with Center for Healthcare Robotics, the Korea Institute of Science and Technology (KIST), Seoul, Republic of Korea. Now he is with the Intelligence and Interaction Research Center of Advanced Materials and Systems Research Division, KIST, since 2024. He has been an Assistant Professor with the Department of AI-Robotics, University of Science and Technology (UST)-KIST School concurrently since 2018. His research interests include bio-inspired robots, smart materials and structures-based soft robotic mechanisms, and wearable devices.

Kyu-Jin Cho (Member, IEEE) received the B.S. and M.S. degrees in mechanical engineering from Seoul National University, Seoul, Republic of Korea, in 1998 and 2000, respectively, and the Ph.D. degree in mechanical engineering from the Massachusetts Institute of Technology, Cambridge, MA, USA, in 2007.

He was a Postdoctoral Fellow with Harvard Microrobotics Laboratory, Cambridge, MA, USA, until 2008. He is currently a Professor of mechanical engineering, the Director of BioRobotics Laboratory, and the Director of Soft Robotic Research Center with Seoul National University. His research interests include biologically inspired robotics, soft robotics, soft wearable devices, novel mechanisms using smart structures, and rehabilitation/assistive robotics.